

Limited ionicity in poor protic ionic liquids: Association Gibbs energies

Cite as: J. Chem. Phys. **158**, 034507 (2023); <https://doi.org/10.1063/5.0124900>

Submitted: 08 September 2022 • Accepted: 22 December 2022 • Published Online: 18 January 2023

 Devin O. Klapatiuk, Shawn L. Waugh, Abdulrahman A. Mukadam, et al.



View Online



Export Citation



CrossMark

ARTICLES YOU MAY BE INTERESTED IN

[Understanding the physics of hydrophobic solvation](#)

The Journal of Chemical Physics **158**, 034508 (2023); <https://doi.org/10.1063/5.0134060>

[TBMaLT, a flexible toolkit for combining tight-binding and machine learning](#)

The Journal of Chemical Physics **158**, 034801 (2023); <https://doi.org/10.1063/5.0132892>

[Phase diagrams—Why they matter and how to predict them](#)

The Journal of Chemical Physics **158**, 030902 (2023); <https://doi.org/10.1063/5.0131028>



Time to get excited.
Lock-in Amplifiers – from DC to 8.5 GHz

Find out more

 Zurich
Instruments

Limited ionicity in poor protic ionic liquids: Association Gibbs energies

Cite as: J. Chem. Phys. 158, 034507 (2023); doi: 10.1063/5.0124900

Submitted: 8 September 2022 • Accepted: 22 December 2022 •

Published Online: 18 January 2023



View Online



Export Citation



CrossMark

Devin O. Klapatiuk,^{a)}  Shawn L. Waugh, Abdulrahman A. Mukadam, and Allan L. L. East^{b)} 

AFFILIATIONS

Department of Chemistry and Biochemistry, University of Regina, Regina, Saskatchewan S4S0A2, Canada

^{a)}Current address: Department of Chemistry, University of British Columbia, Vancouver, British Columbia V6T 1Z1, Canada.

^{b)}Author to whom correspondence should be addressed: allan.east@uregina.ca

ABSTRACT

Protic ionic liquids (PILs), made from anhydrous mixtures of Bronsted acids HA and bases B ($\text{HA} + \text{B} \rightarrow \text{BH}^+ + \text{A}^-$), occasionally suffer from limited ionicity. In cases of “poor” PILs (<10% ionicity, e.g., using carboxylic acids), past simulations have hinted that ion-pair association, more than incomplete proton transfer, is at fault. To improve upon the Fuoss equation for predicting the degree of ion pairing, new electrostatic equations (including induced dipoles) are presented, for ion-pair and other associations that occur in anhydrous amine/carboxylic acid mixtures. The equations present the association Gibbs energies ΔG_A (and thus the association constants K_A) as functions of three fundamental properties: the acid/base mixing ratio ($n = x_A/x_B$), the HA-to-B proton-transfer strength ($\Delta pK_{a,\epsilon=78}$), and the dielectric constant (relative permittivity) of the mixture (ϵ). Parameter values were obtained from fits to constant-dielectric quantum chemistry data (obtained and presented here). These ΔG_A functions were then used to predict ΔG_{ioniz} values for the net ion-generating (autoionization) equilibrium in carboxylic acid/amine mixtures: $2 \text{B}(\text{HA})_n \rightleftharpoons \text{B}(\text{HA})_{n-d}\text{HB}^+ + \text{A}(\text{HA})_{n+d-1}^-$, where $n = x_A/x_B$ and $d = \text{degree of disproportionation}$. The agreement with experiment was excellent, demonstrating that these equations could have useful predictive power.

Published under an exclusive license by AIP Publishing. <https://doi.org/10.1063/5.0124900>

I. INTRODUCTION

A. Limited ionicity in PILs

Protic ionic liquids (PILs) are ionic liquids creatable by anhydrous mixing of Bronsted acids with Bronsted bases, generating high ion concentrations via proton transfer.¹⁻⁴ An important property of ionic liquids, especially for electrolyte purposes, is the degree of ionicity,^{5,6} taken here to be $\alpha = \sigma/\sigma_{\text{ideal}} = \Lambda/\Lambda_{\text{ideal}}$, where σ and Λ are, respectively, the specific (S cm^{-1}) and equivalent or molar ($\text{S cm}^2 \text{mol}^{-1}$) ionic conductivities. The present paper aims to assist the research goals of understanding and quantitatively predicting the ionicity of poor PILs, having less than 10% ionicity.

Ideal conductivity in liquids has been variously defined, usually with the sense that it should be limited only by viscosity η or the presumably viscosity-controlled ion self-diffusion coefficients D_j . The usual η -limited choice for Λ_{ideal} is Angell's⁷ simple Walden-plot choice of $\Lambda_{\text{ideal}} = \Lambda_{\eta,\text{AW}} = \eta^{-1}$ although there is also the adjusted choice $\Lambda_{\eta,\text{MW}} = \eta^{-1} (1/r^+ + 1/r^-)$ by MacFarlane *et al.*⁵; in both cases, the units for Λ_{ideal} are $\text{S cm}^2 \text{mol}^{-1}$ if η is in Poise and the ion radii r are in Angstroms. Angell's ionicity metric⁷⁻⁹

$\Delta \hat{W} = \log \eta^{-1} - \log \Lambda$,⁷ which can be converted into an ionicity via $\alpha_{\eta,\text{AW}} = 10^{-\Delta \hat{W}}$ or $\alpha_{\eta,\text{MW}} = 10^{-\Delta \hat{W}} (1/r^+ + 1/r^-)^{-1}$, if $\Lambda_{\text{ideal}} = \Lambda_{\eta,\text{AW}}$ or $\Lambda_{\eta,\text{MW}}$, respectively. As for D_j -limited choices for Λ_{ideal} , the usual one is the Nernst-Einstein equation $\Lambda_{\text{ideal}} = \Lambda_{\text{D,NE}} = (F^2/RT) \sum \{z_j^2 v_j D_j\}$, where F is Faraday's constant and z_j and v_j are the integer charge and the stoichiometric number of ion type j . The Watanabe^{6,10-12} ionicity metric $\Lambda/\Lambda_{\text{nmr}}$ is $\alpha_{\text{D,NE}}$, while Hansen and MacDonald's¹³ $\Delta = (\sigma_{\text{D,NE}} - \sigma)/\sigma_{\text{D,NE}}$ converts to $\alpha_{\text{D,NE}} = 1 - \Delta$, and the Haven ratio¹⁴⁻²⁰ $H_R = \Lambda_{\text{D,NE}}/\Lambda$ converts to $\alpha_{\text{D,NE}} = H_R^{-1}$.

Table I lists the ionicities $\alpha_{\eta,\text{AW}}$ and $\alpha_{\text{D,NE}}$ of several ionic liquids, including four PILs. Note that the $\alpha_{\eta,\text{AW}}$ and $\alpha_{\text{D,NE}}$ values are rather similar, as has been found in other ionic liquid studies.^{12,21} Harris noted that the two values diverge dramatically for some simple molten salts, with $\alpha_{\eta,\text{AW}}$ values becoming large.²² This divergence is due to the divergence of the two ideals, the viscosity and diffusion-constant limits: one ion is *supermobile*, with its diffusion-constant limit escaping its viscosity limit. From the data presented by Harris, it seems to be appearing in cases with an ion size mismatch (the small cations Li^+ , Na^+ , Cu^+).

TABLE I. Limited ionicities α of room-temperature ionic liquids from experimental data.^{a,b}

Ionic liquid	ΔpK_a	Λ	η	η^{-1}	$\Delta \hat{W}$	$\alpha_{\eta,AW}$	$\alpha_{D,NE}$	References
emim (CF ₃ SO ₃) ₂ N		2.7 ^c	27	3.7	0.14 ^c	0.73 ^c	0.75 ^c	Tokuda <i>et al.</i> (30 °C) ¹¹
bmim PF ₆		0.40	182	0.5	0.14	0.73	0.68	Tokuda <i>et al.</i> (30 °C) ¹¹
bmim (CF ₃ SO ₃) ₂ N		0.64	87	1.2	0.25	0.56	0.63	Tokuda <i>et al.</i> (30 °C) ¹¹
bpyr (CF ₃ SO ₃) ₂ N		1.2 ^d	49	2.0	0.23 ^d	0.59 ^d	0.63 ^d	Tokuda <i>et al.</i> (30 °C) ¹¹
dema CF ₃ SO ₃	22				0.21	0.62	0.61	Davidowski <i>et al.</i> ⁸
bmim CF ₃ SO ₃		0.80	64	1.6	0.29	0.51	0.57	Tokuda <i>et al.</i> (30 °C) ¹¹
bmim CF ₃ COO		0.80	58	1.7	0.33	0.46	0.52	Tokuda <i>et al.</i> (30 °C) ¹¹
dema CH ₃ SO ₃	12				0.37	0.43	0.33	Davidowski <i>et al.</i> ⁸
dema CF ₃ COO	10				0.83	0.15	0.23	Davidowski <i>et al.</i> ⁸
dema CH ₃ COO	6				1.75	0.02	0.05	Davidowski <i>et al.</i> ⁸

^aUnits: Λ in S cm² mol⁻¹; η in cP; η^{-1} in P⁻¹.

^b $\alpha_{\eta,AW}$ (Angell–Walden) assumes $\Lambda_{ideal} = \eta^{-1}$, while $\alpha_{D,NE}$ assumes $\Lambda_{ideal} = \Lambda_{D,NE}$. The $\Delta \hat{W}$ column is Angell's ionicity metric (see the text).

^cLower conductivities reported earlier¹⁰ produce $\{\Lambda, \Delta W, \alpha_{\eta,AW}, \alpha_{D,NE}\} = \{1.8, 0.30, 0.50, 0.45\}$.

^dLower conductivities reported earlier¹⁰ produce $\{\Lambda, \Delta W, \alpha_{\eta,AW}, \alpha_{D,NE}\} = \{0.9, 0.35, 0.45, 0.40\}$.

Limited ionicity ($\alpha < 1$) is due to additional limitations beyond viscosity or diffusion coefficients. Relative to a Nernst–Einstein ideal, the reasons for limited ionicity ($\alpha_{D,NE} < 1$) are ion–ion correlations beyond those already present in the diffusion coefficients,²³ and a review of some older literature may help to give some clarity here.

The phenomenon of deviations from the Nernst–Einstein ideal seems to have gained awareness in the 1950s from radiotracer experiments; an early example was the 1956 Compton result for AgCl crystals ($\alpha = 1.7$, $H_R = 0.6$, “superionic”).²⁴ Taking a 1952 proposal from Bardeen and Herring (Bardeen, a future two-time Nobel laureate),²⁵ Compaan and Haven^{14,15} pursued explanations for an inhibition factor f limiting diffusion (not conductivity) based on random walk models with correlated steps, not realizing that such correlations would also limit conductivity as well. In 1971, Sato and Kikuchi,^{26,27} studying β and β'' -alumina, improved the model by introducing a second inhibition factor f_I limiting conductivity, and proposing random-walk-based ideals for both D and σ : $D = f D_{ideal}$, $\sigma = f_I \sigma_{ideal}$, and hence $\alpha = D_{\sigma,NE}/D = f_I/f$, with a model for predicting f and f_I . For example, for β -alumina with a sodium ion concentration (site coverage) of 0.6, they predicted $f = 0.45$, $f_I = 0.58$, and $\alpha = 1.3$,²⁶ meaning that though the conductivity appears limited from their random-walk-based ideal, the cation diffusion is limited to a somehow greater extent, resulting in the “superionicity” ($\alpha > 1$, $H_R < 1$) relative to the Nernst–Einstein diffusion-constant-limited ideal. In the liquid state, however, deviations from a Nernst–Einstein ideal are generally “subionic” ($\alpha < 1$, $H_R > 1$); an early molten salt example is the 1956 result of Borucka *et al.* for molten NaCl at 935 °C ($\alpha = 0.7$, $H_R = 1.4$).²⁸

The best explanation we have yet found for how ion correlation is limiting diffusion and conductivity differently is in the 1993 report of Lonergan *et al.*¹⁷ They used Monte Carlo lattice gas modeling; Table II provides an exemplary subset of their results.

Their first case (SISM, single ion singly mobile), having no counterion attractions, isolates like-ion correlation effects. This model produced $f < 1$ (diffusion inhibition) but $f_I > 1$ (conductivity enhancement), explained by Lonergan *et al.* as due to the

like-ion repulsions hindering single-ion diffusion but pushing forward its ion cloud, resulting in a net conductivity enhancement. Their next case (DISM, dual-ion singly mobile) correctly reproduced the superionic nature of the solid-state systems, showing that the introduction of counterion attractions greatly reduced both f and f_I (from their SISM values) but maintained $f < f_I$ (and hence H_R remained < 1 , superionic) from the repulsive ion-cloud effects that were isolated in the SISM model. Finally, in their DIDM case (dual-ion doubly mobile), we see that f (but not f_I) has risen somewhat from DISM values. This is due to the ion pairs being now mobile, which increased tracer-ion diffusion but did not affect conductivity, allowing diffusion to now become less limited than the conductivity ($f > f_I$) and causing the appearance of subionic ($H_R > 1$, $\alpha < 1$) behavior.

For the limited ionicity ($\alpha < 1$) of ionic liquids, we think the DIDM-model results of Lonergan *et al.* are apt: that counterion correlation (attractions) are inhibiting ion diffusion, but not as much as they are inhibiting conductivity, due to the likelihood that ion–counterion correlations are causing motions of ion “pairs” that contribute to ion diffusion but not conductivity. Such “paired” motion likely involves nearest neighbors, but opinions have varied on whether to consider this as short-lived ion pairs or complexes^{5,6,8,13,23,28–31} or an ionic-atmosphere (Debye–Huckel–Onsager) effect.^{8,23,30,32–35} Molecular dynamics (MD) computer modeling has been used to probe this question. The classic 1975 result of Hansen and MacDonald¹³ produced limited ionicity ($\alpha \sim 0.8$, $\Delta \sim 0.2$) for a molten salt assuming Coulomb r^{-1} attraction and r^{-9} repulsion between atomic ions.

TABLE II. Lattice gas modeling results¹⁷: anion concentration of 1/40, $T^* = 1/15$.

Model system	$H_R = f/f_I$	f	f_I
SISM (mobile anions, no cations)	0.4	0.75	2.0
DISM (mobile anions, fixed cations)	0.6	0.15	0.25
DIDM (mobile anions and cations)	1.8	0.45	0.25

They stated that “the obvious explanation of deviations from the Nernst–Einstein relation lies in the formation of ionic complexes, which contribute to the diffusive flux but not to the electrical current,” and noted that the nature of the counterion correlations was “short-lived.” Modern PILs of “good” ionicity, composed of polyatomic ions and made from strong acids, have ionicities of ~40%–80% ($\alpha \sim 0.4$ – 0.8 , $\Delta\hat{W} < 0.4$, see Table I), and molecular dynamics simulations of these (e.g., bmim PF₆)³⁰ also show no “long-lived” complexes or ion pairs. Some ion-pairing models place the lifetimes of any given ion pair in the ps-to-ns range,^{30,31} and we agree with Harris³⁵ that when the lifetimes become particularly short (ps?), then the alternative interpretation of ionic-atmosphere effects (such as Klemm/Laity friction coefficients^{32,33}) would have more physical appeal.

One bizarre hypothesis for the instances of mildly reduced ionicity ($\alpha > 50\%$) is that it is due to reduced *charge* on the ions.^{36–41} This hypothesis appears to have arisen from the observation that fractional net charges on polyatomic ions have been used in non-polarizable “fixed-charge” molecular dynamics simulations to cure an underprediction of known ion diffusion coefficients.^{42–44} First, this observation does not support the hypothesis that the employed reduced charges are *causing* the resulting limited ionicity in these simulations, since limited ionicity was already observed in basic MD simulations with full ion charges.¹³ Second, the hypothesis violates the natural expectation that an ion should recover fully intact electrons when leaving an ion pair to transport its charge via translation through a medium toward an electrode.

As for the reasons for limited ionicity relative to the Angell–Walden ideal (ionicities $\alpha_{\eta,AW} < 1$), rather than to the Nernst–Einstein ideal, Table I shows that the α values from the two definitions are generally similar but appear to quantitatively disagree more when the ionicity dips below 50%. It can be shown that Angell’s $\Lambda_{ideal} = \eta^{-1}$ corresponds to $\Lambda_{ideal} = \Lambda_{D,NE}$ if the ions in the ionic liquid have charge $z_j = \pm 1$ and radii $r_j = 1.6$ Å, which is not unreasonable. Interestingly, we see cases where $\alpha_{\eta,AW} > \alpha_{D,NE}$ (e.g., dema CH₃SO₃) and cases where $\alpha_{\eta,AW} < \alpha_{D,NE}$ (e.g., dema CX₃COO cases). In the dema CH₃SO₃ case, it must be that $\Lambda_{ideal,\eta,AW} < \Lambda_{ideal,D,NE}$, i.e., a diffusion constant is larger than expected from the viscosity, indicating a supermobile ion or ion pair that is beating the viscosity limit. In the dema CX₃COO cases, the diffusion coefficients are *smaller* than expected, indicating perhaps ion pairs or aggregates $\gg 1.6$ Å. We recall a published criticism⁴⁵ of Angell’s choice $\Lambda_{ideal} = \eta^{-1}$ on the grounds that he originally justified it as being the conductivity of 1M aqueous KCl, a non-ideal system in the sense of activity (mean activity coefficient of 0.61 at T = 298 K)⁴⁶ as well as Walden-plot slope (a “fractional” Walden rule even when infinitely dilute⁴⁴). We think it likely that Angell meant “ideal” only in the sense that 1M aqueous KCl, like the strong-acid PILs that also lie on that line $\Lambda = \eta^{-1}$, are thought to feature no significant aberrations like ion pairing or ion supermobility. This lack of aberrations and apparently similar Stokes radii (near 1.6 Å) seems to be what allows 1M aqueous KCl and strong-acid PILs to have such similar Walden products ($\Lambda\eta \approx 1$ P S cm² mol⁻¹).

B. Ion complexes in poor PILs

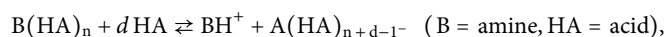
The present paper is concerned with “poor” protic ionic liquids,⁷ defined here as cases of $\alpha < 0.1$ ($\Delta\hat{W} > 1$). Poor PILs include

the classic cases of carboxylic acids with amines, where the conductivities for 1:1 mixtures are so limited that they fall below values seen at non-stoichiometric mixing ratios; a common conductivity maximum at acid mole fractions near $x_B = 0.17$ (1:5 base:acid) has been known for over 100 years.^{47–51} A second maximum of varying location has sometimes been seen as well.^{47,50,51} In 2018, Aravindakshan *et al.* published the first explanations of these conductivity phenomena, based on observations of ion pairs in their *ab initio* molecular dynamics (AIMD) simulations.⁵² The shifted maxima are driven mainly by maximum ion concentrations, which depend on optimal conditions for unpaired-ion stability, namely, high values for the product ϵr_{\pm} of dielectric constant $\epsilon(x_B)$ and polyatomic ion radius $r_{\pm}(x_B)$. In the acetic acid + water case they also examined, the product is maximal near $x_B = 0.94$ due to the high ϵ of water. However, in the acetic acid + pyridine case, the product is maximal near $x_B = 0.17$ due to high effective ion radii r_{\pm} in acid-rich conditions, made possible by the amphoteric nature of carboxylic acids, which allows for homoassociated anions.

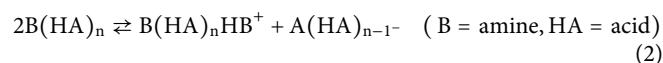
These qualitative explanations arose from the *quantitative* reproduction of the $\sigma(x_B)$ conductivity curves of those two systems, using a Walden’s rule formalism,

$$\sigma(x_B) = W \frac{C_{ions}}{\eta} = W \frac{2\alpha\rho}{M\eta}, \quad (1)$$

and employed experimentally known densities $\rho(x_B)$ and viscosities $\eta(x_B)$, and weighted-average molar masses $M(x_B)$.⁵² Expressions for the Walden constant $W\{r_{\pm}(x_B)\}$, the degree of ionization $\alpha\{\epsilon(x_B), r_{\pm}(x_B)\}$, dielectric constants $\epsilon(x_B)$, and ion radii $r_{\pm}(x_B)$ were needed. Such a model had in fact been applied first by Huyskens *et al.* in 1980 for acid + amine mixtures;⁴⁹ however, they did not predict the degree of ionization from first principles but instead used experimental conductivities to work *backward* to derive ion sizes. Huyskens assumed the ionization equilibrium to be



and derived $d = 1$ from the data. In the model of Aravindakshan *et al.*,⁵² which we shall call the *2018 kite theory*, two new innovations were applied. First, the autoionization reaction was modernized to be



which employs the simulation-revealed^{52,53} *triple-ion*^{54,55} complex cations $B(HA)_n HB^+$ *in lieu* of the historically assumed BH^+ monomer cations. [“Kite” refers to the $B(HA)_n$ structures.] Second, for $\alpha\{\epsilon(x_B), r_{\pm}(x_B)\}$, an association constant approximation, the Fuoss equation,⁵⁶ was employed to allow *forward* computation of conductivity starting from ion radii $r_{\pm}(x_B)$. Only two fitting parameters were needed (to account for the difficult-to-define ion sizes) to reproduce $\sigma(x_B)$.

The 2018 kite theory worked well for pyridine + acetic acid, but it was reported that the same theory applied to acetic acid + triethylamine needed unrealistic ion sizes.⁵² We suspected that its use of the Fuoss approximation was not generating enough ions (“overbinding the ion pairs”) when triethylamine was the base. The Fuoss equation⁵⁶ in modern (non-cgs) units⁵² is

$$K_A = K_{A,\infty} e^b, \quad (3)$$

$$K_{A,\infty} = (4/3)\pi a^3 N_{AVO} c^*, \quad (4)$$

$$b = \epsilon_0^2 / (4\pi\epsilon_0\epsilon a kT), \quad (5)$$

for ion-pair association. It takes fixed values for the usual fundamental constants k , e_0 , ϵ_0 , N_{AVO} (Avogadro's number), and standard concentration $c^* = 1 \text{ mol dm}^{-3}$, and requires only the dielectric constant ϵ , the contact distance a in the associated ion pair, and the temperature T . Among a variety of assumptions made in the 2018 application that could be problematic are (i) that the dielectric constant ϵ depends linearly on the mass fraction of component B, (ii) that non-ionic (e.g., covalent or polarization) effects are negligible during ion pairing, (iii) that Eq. (2) is the only ion-generating equilibrium, and (iv) that the Fuoss equation could be applied directly to Eq. (2). Equation (2), the overall autoionization reaction, is a sum of two steps: ion-pair (+−) dissociation $B(\text{HA})_n \rightleftharpoons \text{HB}^+ + A(\text{HA})_{n-1}^-$ (for which the Fuoss equation is most relevant), and a cation complexation (+0) step $B(\text{HA})_n + \text{HB}^+ \rightleftharpoons B(\text{HA})_n\text{HB}^+$. The way the Fuoss equation was applied for K_{ioniz} in 2018⁵² was equivalent to assuming, in $K_{\text{ioniz}} = K_{D,+} K_{A,+0} = K_{A,+0}/K_{A,+}$, that $K_{A,+0} = 1000$ and $K_{A,+} = K_{A,\text{Fuoss}}$.

To test those Fuoss-generated K_{ioniz} and ΔG_{ioniz} values, “experimental” values were derived from known conductivities and viscosities for six systems and many mole fractions x_B , using Eq. (1) to derive α , followed by $K_{\text{ioniz}} = \alpha^2 / (x_i - 2\alpha)^2$ and $\Delta G_{\text{ioniz}} = -RT \ln K_{\text{ioniz}}$.⁵³ The results showed that $K_{\text{ioniz,expt}}$ is indeed maximal ($\Delta G_{\text{ioniz,expt}}$ is minimal) near $x_B = 0.16$ – 0.20 generally,⁵³ as the Fuoss equation was predicting.⁵² What was not done at the time was to explore how these $K_{\text{ioniz,expt}}$ (or $\Delta G_{\text{ioniz,expt}}$) values could be used to improve upon the Fuoss equation for their general prediction.

The current paper improves the 2018 version of kite theory by replacing the Fuoss equation for prediction of ΔG_{ioniz} (and hence K_{ioniz} , α , and conductivity σ) as a function of mole ratio $n = x_A/x_B$, dielectric constant ϵ , and relative acid/base strength of components ΔpK_a . It first reports a set of training data obtained with constant-dielectric quantum-chemistry computation: values of ΔG_A for four types of associations, as well as the net ΔG_{ioniz} for Eq. (2), computed for HA = acetic acid paired with four different amines B. It then

reports the new summary equations, with comparison to the older equation of Fuoss.

II. METHODOLOGY

Gaussian 09⁵⁷ was used to optimize the geometries and compute the energies of several hydrogen-bonded complexes: the homoassociated anions $A(\text{HA})_{n-1}^-$, the “ion-pair” neutrals $B(\text{HA})_n$, and the “triple-ion” cations $B(\text{HA})_n\text{HB}^+$. The quantum chemistry ESM (electronic structure methods) used were B3LYP/6-31+G(d,p) and M06-2X/6-31+G(d,p). Geometry optimizations were performed with B3LYP in three solvation environments: the gas phase (equivalent to a dielectric constant $\epsilon = 1$), and with SCRFF (solvent = acetic acid) and SCRFF (solvent = water), which employ $\epsilon = 6.2528$ and 78.3553 , respectively, within Gaussian 09's default continuum solvation model (CSM), IEFPCM^{58,59} with UFFx1.1 cavity radii.⁶⁰ The acid HA was taken to be acetic acid only, and four bases B were examined: pyridine (pyr), methylimidazole (mim), 1,4-diazabicyclo[2.2.2]octane (dab), and triethylamine (tea), having experimentally known (at 25 °C) pK_a values of 5.2, 7.0, 8.7, and 10.8, respectively.⁴⁶ Complexes of up to $n = 5$ acetate units were computed.

As usual, the CSM-specific Gibbs energy computation for 1M concentration is⁶¹

$$\begin{aligned} G^* &= G_{\text{gas}}^\circ + \Delta G^{\circ \rightarrow *}_G + \Delta_{\text{solv}} G^* \\ &= E_{\text{el,gas}} + G_{\text{freq}}^\circ + \Delta G^{\circ \rightarrow *}_G + \Delta_{\text{solv}} G^* \\ &= G_{\text{el,e}}^* + G_{\text{freq}}^\circ + \Delta G^{\circ \rightarrow *}_G, \end{aligned} \quad (6)$$

where $^\circ$ indicates gas-phase standard-state conditions of $T^\circ = 298 \text{ K}$ and $P^\circ = 1 \text{ atm}$. $\Delta G^{\circ \rightarrow *}_G$ is the cratic (concentration-change) term $RT \ln (c^*/c^\circ) = RT \ln ([1M]/[P^\circ/RT^\circ]) = +1.89 \text{ kcal mol}^{-1}$. G_{freq}° is the set of thermal motion (nuclear-motion degree-of-freedom) corrections, including zero-point vibrational energy, to convert the electronic energy $E_{\text{el,gas}}$ to Gibbs energy G_{gas} , typically done with single-conformer vibrational frequency calculations that employ gas-phase rigid-rotor harmonic-oscillator equations and assume by default 1 atm gas concentrations. $\Delta_{\text{solv}} G^*$ is the constant-concentration solvation Gibbs energy determined by the

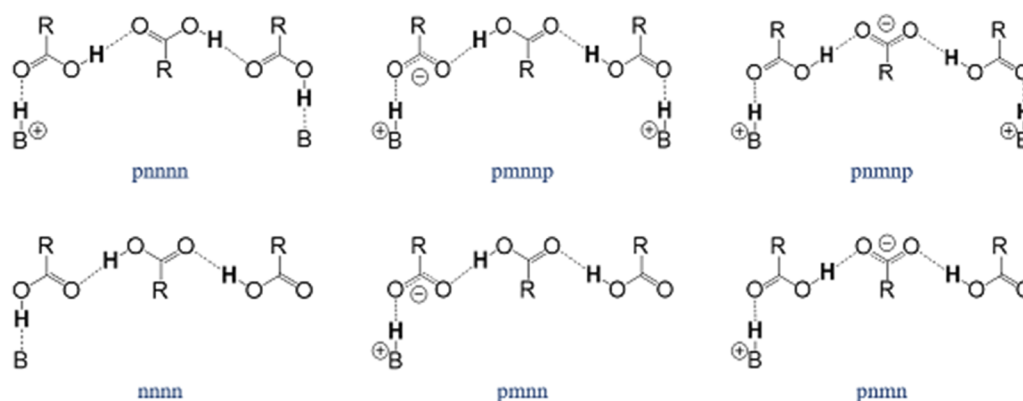


FIG. 1. Proton-transfer isomer possibilities for $B(\text{HA})_3\text{HB}^+$ (top) and $B(\text{HA})_3$ (bottom). The $B(\text{HA})_n$ complexes are referred to as kites, with an amine head and an acid tail.

CSM calculation. A Gaussian 09 SCRF frequency run reports a Gibbs energy that is conventionally understood to be only the sum $G_{el,\epsilon}^* + G_{freq}^0$, and thus the researcher must add the $\Delta G^{0 \rightarrow *}$ = +1.89 kcal mol⁻¹ term *a posteriori*. We used the B3LYP opt+freq run for G_{freq}^0 and the M06-2X single-point run for $G_{el,\epsilon}^*$.

The Gibbs energies of reaction [association and Eq. (2) autoionization] are plotted vs the number *n* of acetate groups in the kite; the relation between the expected kite length and the mixing mole fractions x_{Acid} and x_{Base} is $n = x_A/x_B$, the mixing ratio.

Obtaining a systematic set of optimized single conformers was arduous work. There were multiple *proton-transfer* and *rotamer* (dihedral-angle) possibilities. Some examples of proton-transfer possibilities appear in Fig. 1. The rotamer issues were particularly challenging (supplementary material), due to (i) the extremely flat potential energy surfaces for the floppy long H-bonded chains, (ii) the surprising number of imaginary frequencies obtained for the hypothesized C_s -symmetry structures, forcing one to choose among several C_1 -symmetry minima (from various acetate and methyl dihedral-angle distortions), and (iii) the imprecision in obtaining these distortions correctly when dealing with discretized grids from both SCRF (cavity tesserae) and B3LYP (numerical integration grid). In the end, all H-bonded complexes except the rotationally symmetric BHB⁺ ions pyr·H⁺·pyr and dab·H⁺·dab were obtained from C_1 -symmetry optimizations (to ensure all vibrational modes contribute to Gibbs energy) and with the “nosymm” flag (to avoid an axis rotation approximation with SCRF-cavity geometry optimizations of nearly-symmetric structures⁶²).

III. QUANTUM CHEMISTRY RESULTS

A. Nature of complexes

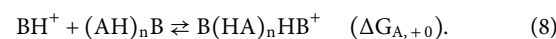
The predicted preferred proton-transfer isomers are listed in Table III for the “ion pairs” B(HA)_{*n*} and Table IV for the “triple-ion” cations B(HA)_{*n*}HB⁺. It is seen that the “ion pairs” and “triple ions” are not always so: in some instances, the amine unit is

unprotonated, too weak to draw H⁺ from the acid units. The results show that “ion pairs” have an increasing tendency to exist in an all-neutral state with decreasing ϵ , decreasing basicity (pK_a) of the base, and decreasing size *n* of the complex. The same is true for the conditions where “triple ions” have an increasing tendency to exist as a complex single ion.

We observed a somewhat smooth dependence of association energies vs any of these underlying properties (ϵ , pK_a, *n*). Energetically, the all-neutral cases of B(HA)_{*n*} need at most only 2 kcal mol⁻¹ extra energy to achieve the proton transfer needed to create the ion pair [BH⁺][(AH)_{*n*}A⁻]; this is a minor fraction of the total dissociation energy (into separated ions) in these cases. It seems reasonable to continue using the term “ion pairs” and “triple ions” for the neutral and cationic complexes, regardless of the actual protomer that is most stable at a particular ϵ , pK_a, and *n*.

B. BH⁺ associations

Figure 2 plots the computed association Gibbs energies for associating BH⁺ via hydrogen bond to an anionic tail [ion pairing, Eq. (7)] or an existing ion-pair kite [cation complexation, Eq. (8)], plotted against the number of acetate units in the tail,



The ion pairing energies (left-hand plot) are seen to rise (become less favorable) with increasing ϵ , increasing *n*, and increasing basicity (pK_a) of the base, since these increases all lead to increased stability of the reactants (ions). In the *dfd* limit of infinite dielectric (black to red to blue and beyond), the energies rapidly rise toward a positive Gibbs-energy ceiling, possibly an entropy-only ceiling, which we estimate to be ≈+5 kcal mol⁻¹ for hydrogen-bond associations in liquid phases (see Sec. IV). Any

TABLE III. Most stable proton-transfer isomers (see Fig. 1 for notation) of “ion-pair” complexes B(HA)_{*n*}.^a

Base, ϵ	Base pK _a	ϵ	[BHA]	[B(HA) ₂]	[B(HA) ₃]	[B(HA) ₄]	[B(HA) ₅]
tea, in H ₂ O	10.75	78.3553	pm	pmn	pmnn	pnmnn	pnmnnn
dab, in H ₂ O	8.7	78.3553	pm	pmn	pmnn	pnmnn	pnmnnn
mim, in H ₂ O	6.95	78.3553	nn	pmn	pmnn	pnmnn	pnmnnn
pyr, in H ₂ O	5.23	78.3553	nn	pmn	pmnn	pmnnn	pmnnnn
tea, in AA	10.75	6.2528	nn	pmn	pmnn	pmnnn	pmnnnn
dab, in AA	8.7	6.2528	nn	pmn	pmnn	pmnnn	pmnnnn
mim, in AA	6.95	6.2528	nn	nnn	pmnn	pmnnn	pmnnnn
pyr, in AA	5.23	6.2528	nn	nnn	nnnn	nnnnn	nnnnnn
tea, in gas	10.75	1	nn	nnn	pmnn	pmnnn	pmnnnn
dab, in gas	8.7	1	nn	nnn	nnnn	nnnnn	nnnnnn
mim, in gas	6.95	1	nn	nnn	nnnn	nnnnn	nnnnnn
pyr, in gas	5.23	1	nn	nnn	nnnn	nnnnn	nnnnnn

^aFrom B3LYP/6-31+G(d,p)/SCRF optimization. The pK_a values are 25 °C values from the CRC Handbook.⁴⁶ The dielectric constant values ϵ are those used by Gaussian 09.⁵⁷ Boldface denotes an unprotonated amine in the complex.

TABLE IV. Most stable proton-transfer isomers (see Fig. 1 for notation) of “triple-ion” complexes $B(HA_n)HB^+$.^a

Base, ϵ	Base pK_a	ϵ	[BHAHB ⁺]	[B(HA) ₂ HB ⁺]	[B(HA) ₃ HB ⁺]	[B(HA) ₄ HB ⁺]	[B(HA) ₅ HB ⁺]
tea, in H ₂ O	10.75	78.3553	pmp	pmnp	pnmnp	pnmnp	pnmnp
dab, in H ₂ O	8.7	78.3553	pmp	pmnp	pnmnp	pnmnp	pnmnp
mim, in H ₂ O	6.95	78.3553	pmp	pmnp	pnmnp	pnmnp	pnmnp
pyr, in H ₂ O	5.23	78.3553	pmp	pmnp	pnmnp	pnmnp	pnmnp
tea, in AA	10.75	6.2528	pmp	pmnp	pnmnp	pnmnp	pnmnp
dab, in AA	8.7	6.2528	pmp	pmnp	pnmnp	pnmnp	pnmnp
mim, in AA	6.95	6.2528	pmp	pmnp	pnmnp	pnmnp	pnmnp
pyr, in AA	5.23	6.2528	pmp	pmnp	pnmnp	pnmnp	pnmnp
tea in gas	10.75	1	pmp	pmnp	pnmnp	pnmnp	pnmnp
dab, in gas	8.7	1	pmp	pmnp	pnmnp	pnmnp	pnmnp
mim, in gas	6.95	1	pnn	pnnn	pnnnn	pnnnnn	pnnnnnn
pyr, in gas	5.23	1	pnn	pnnn	pnnnn	pnnnnn	pnnnnnn

^aFrom B3LYP/6-31+G(d,p)/SCRF optimization. The pK_a values are 25 °C values from the CRC Handbook.⁴⁶ The dielectric constant values ϵ are those used by Gaussian 09.³⁷ Boldface denotes an unprotonated amine in the complex.

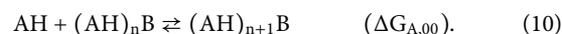
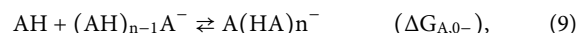
downward displacement from this +5 ceiling would be enthalpic and appears to be roughly proportional to $1/\epsilon$, as expected from Coulomb's law.

The cation complexation energies (right-hand plot) reveal clear benefits to complexation in the gas phase predictions ($\epsilon = 1$), with ΔG_A becoming as much as -30 kcal mol⁻¹, but for $\epsilon > 5$ dielectric environments, they become very mild and almost constant with n , as we had been assuming.⁵² The entropic ceiling of $+5$ kcal mol⁻¹ would again apply to these data, in the limit of infinite dielectric. Note that in the limit of infinite kite tail length n , these complexation energies do *not* tend to $+5$, best revealed in the $\epsilon = 1$ cation complexation data. The nonzero enthalpic (ΔH_A) benefits to complexation must therefore exist in a finite dielectric at infinite n and appear to depend on both ϵ and the basicity of the base, which is to be expected of an effect likely dominated by polarization. These n -asymptotes should probably exist, at the same values, for the ion-pair associations (left-hand plot), since as n

becomes infinite, the anion charge becomes infinitely diluted and the chemical nature of the far end becomes immaterial. We thus chose to build such common asymptotes into the summary fitting function (see Sec. IV).

C. HA associations

Figure 3 plots the computed association Gibbs energies for associating HA (acetic acid) via hydrogen bond to an anionic tail [anion growth, Eq. (9)] or an existing ion-pair kite [neutral growth, Eq. (10)], plotted against the number of acetate units in the tail,



The anion growth energies (left-hand plot) are seen to rise (become less favorable) with increasing ϵ and increasing n . The

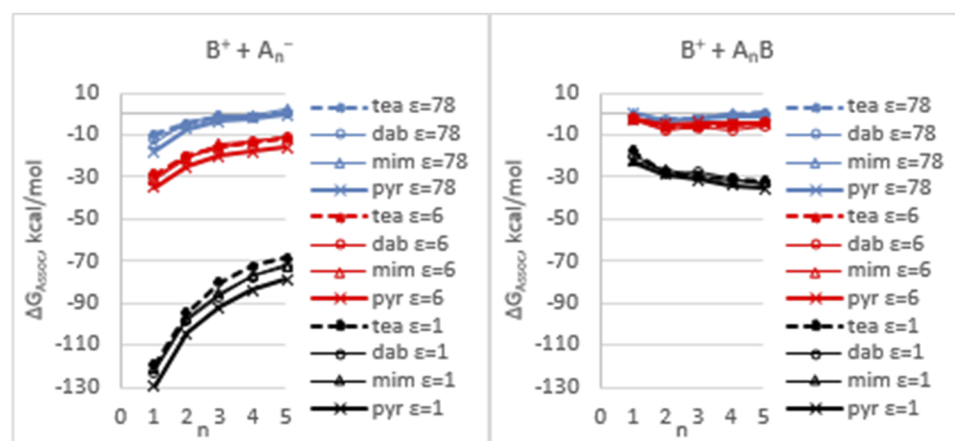


FIG. 2. Computed results for ΔG_A for the BH^+ associations [Eqs. (7) and (8)]. The four amines employed were tea \rightarrow dab \rightarrow mim \rightarrow pyr in the order of decreasing basicity. The figure legends round off the dielectric constant values actually used in the computation (78.3553 and 6.2528).

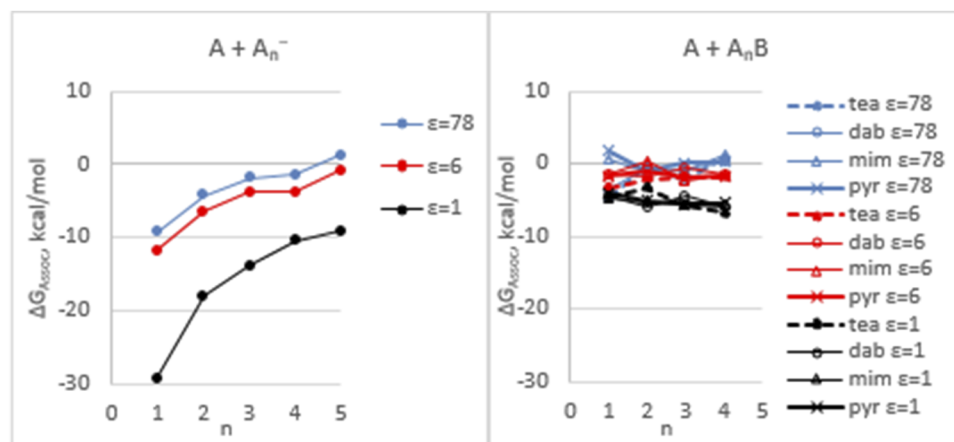


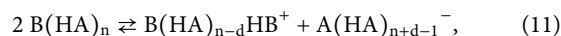
FIG. 3. Computed results for ΔG_A for the HA associations [Eqs. (9) and (10)]. For legend details, see Fig. 2.

trend with increasing dielectric (from black to red to blue and beyond) is again toward the hydrogen-bond association ceiling near $+5 \text{ kcal mol}^{-1}$. In neutral growth (right-hand plot), the association (hydrogen-bond) strength is quite independent of the chain length but does depend on the dielectric constant, and n -asymptotes below 5 kcal mol^{-1} are clearly seen. We again assume that the n -asymptotes in the right-hand plot (one for each ϵ value) must match those of the left-hand plot (see Sec. IV).

D. Autoionization

Values for ΔG_{ioniz} for the ion-controlling equilibrium in Eq. (2) were next computed, to compare to such values obtained from experimental conductivities and viscosities for the $B = \text{tea}$ and

$B = \text{pyr}$ cases.⁵² However, we also considered the possibility of kite tail disproportionation to generate longer anions, motivated both by the $d = 1$ result of Huyskens *et al.*⁴⁹ (mentioned in the Introduction) as well as the ion sizes observed in simulations.^{52,53} We thus broadened the Eq. (2) assumption to become



to allow for $d > 0$ possibilities. Thus, we show in Fig. 4 plots of computed net reaction energies ΔG_{ioniz} for Eq. (11), computed with three different levels of disproportionation ($d = 0, 1, \text{ or } 2$). Interestingly, disproportionation (particularly $d = 1$, i.e., $\Delta G1$, the “plus” symbols in figure) is predicted to be favorable (lowest energy) most often.

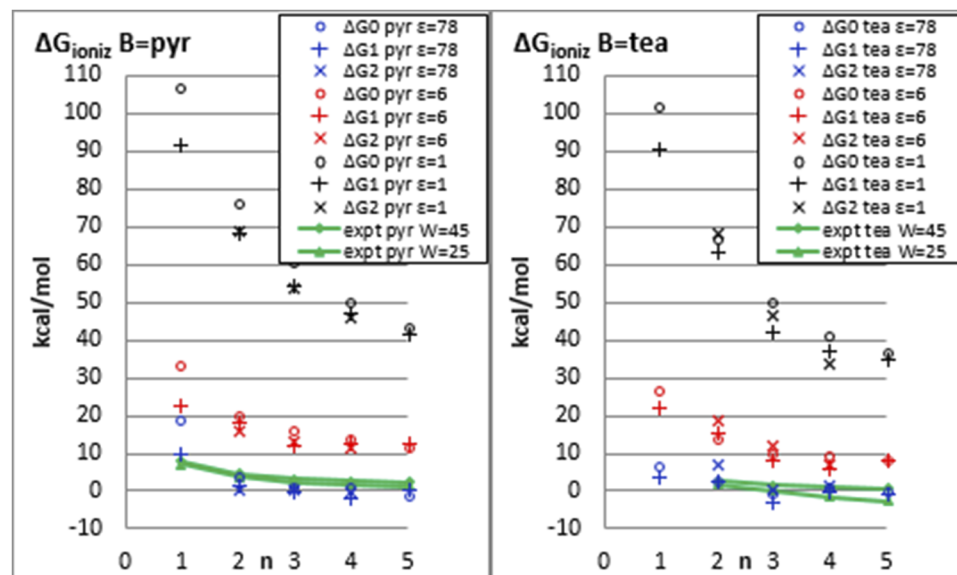


FIG. 4. Computed results for net reaction Gibbs energy ΔG_{ioniz} [Eq. (11)]. The points $\Delta G0$, $\Delta G1$, and $\Delta G2$ refer to $d = 0$, $d = 1$, and $d = 2$ levels of disproportionation; note that $\Delta G1$ is predicted most often to be the lowest-energy option of the three. Values derived from experimental data⁵³ (green lines) are also shown.

A general decrease in the computed ΔG_{ioniz} values with increasing ϵ and kite length n is seen. It is due to the increased stabilization of the products (ions). It is difficult to see any dependence of ΔG_{ioniz} upon the basicity of the base (tea \rightarrow pyr, left plot \rightarrow right plot) when $\epsilon > 5$, but at $\epsilon = 1$, we see slightly lower ΔG_{ioniz} (thus more ionic tendency) for the stronger base (tea). Such a trend is also evident in the data derived from the experiment⁵³ (green curves), where the actual dielectric constant values are uncertain but expected to be between 6 (red points) and 78 (blue points).^{49,63,64} Given that >5 kcal mol⁻¹ absolute errors were expected from the continuum solvation model, especially for ions, the absolute agreement with the experiment is somewhat fortunate. Importantly, there is no serious qualitative disagreement between the quantum-chemistry computed values for ΔG_{ioniz} and the conductivity-derived experimental values, providing more support for the equilibrium assumed [Eq. (11)].

The quantum-chemistry data reveals the explicit dependence on the dielectric constant, which is substantial. The general decline (as n increases) in the ΔG_{ioniz} values derived from experimentally determined conductivities is mimicked by the *constant- ϵ* computed curves, which decline due to the increasing size of the product ions (causing rising ion stability). Thus, the earlier proposal⁵³ that this ΔG_{ioniz} decline is due to the increasing ϵ (due to increasing “kite” lengths, which have larger dipoles) is perhaps not the principal reason. However, in contrast, a decreasing ϵ is likely to be the explanation for the general *rise* in ΔG_{ioniz} at more extreme acid:base ratios beyond 5:1 (as seen in the experimental data⁵³): such a reduced dielectric constant is known,^{63,64} and due to the kite concentration becoming swamped by acid dimer concentration, which must start to become substantial at some point beyond 5:1 mixing ratios.

As a side issue, we note that the computed data are insufficiently accurate to assist in determining the appropriate W (Walden constant) value for deriving the experimental ΔG_{ioniz} .⁵³ The more realistic of the two provided choices of Walden constant W is probably 25, which produces negative ΔG_{ioniz} values in the case $B = \text{tea}$. Given, however, that the creation of charge generally requires work, it is not easy to rationalize negative ΔG_{ioniz} values for an autoionization of $2 \rightarrow 2$ stoichiometry [Eqs. (2) or (11)]. The computed ΔG_{ioniz} values (blue symbols) also show some negative values for large ions ($n > 3$), but only due to the noisy G_{freq} terms; negative values do not arise from the electronic ($G_{\text{el,e}}$) terms alone. The experimental result may be indicative of some free BH^+ monomer present, if the base is tea or stronger; this possibility shall be explored in future work.

IV. THEORY: ASSOCIATION GIBBS ENERGIES

A. Fuoss equation

Armed with the quantum-chemistry computed ΔG_A and ΔG_{ioniz} data, we now develop theoretical expressions for them as functions of ϵ (dielectric constant), n (acid/base mole ratio and thus kite length), and ΔpK_a (acid-to-base proton-transfer strength). As an example and a reference point for the four types of associations [Eqs. (7)–(10)], consider the Fuoss equation [Eq. (3)] for the K_A for the ion-pair association [Eq. (7)]. Since $K = e^{-\Delta G/RT} = e^{\Delta S/R} e^{-\Delta H/RT}$, the Fuoss equation is equivalent to the choices

$$\Delta H_A^{\text{Coulomb}} = N_{\text{AVO}} u_{\text{Coulomb}}, \quad u_{\text{Coulomb}} = -e_0^2 / (4\pi\epsilon_0\epsilon r_{\pm}), \quad (12)$$

$$\Delta S_A^{\text{Fuoss}} = R \ln(V_{\text{pairs}}/V^*), \quad V_{\text{pairs}} = N_{\text{AVO}}(4/3)\pi a^3, \quad (13)$$

where V^* is the inverse of standard concentration (hence 1000 ml mol⁻¹), V_{pairs} is the volume of a mole of ion pairs, a is the radius of the associated pair, and r_{\pm} is the center-to-center ion-pair distance when paired (associated). Fuoss assumed the a in the entropy equals r_{\pm} in the enthalpy.⁵⁶

B. Entropy of association ΔS_A

The entropy from the Fuoss K_A [Eq. (13)] is equivalent to assuming that association results in only a reduction of three translational mode entropies via restricting the translation of one reactant from standard solute volume (1000 ml mol⁻¹) to a smaller volume, V_{pairs} , the volume of a mole of ion-pair spheres. Since $a \geq 3$ Å, then by Eq. (13) $V_{\text{pairs}} \geq 68$ ml mol⁻¹, $\Delta S_A^{\text{Fuoss}} \geq -5.4$ cal mol⁻¹ K⁻¹, and $-\Delta S_A^{\text{Fuoss}} \leq +1.6$ kcal mol⁻¹. We refer to $-\Delta S_A$ as the “entropy ceiling” for ΔG_A (Sec. III B), the value for ΔG_A in the limit of zero enthalpic benefit for association. This ceiling now appears to be too low. The B3LYP SCRF calculations, which employ quantum mechanical entropy predictions, reveal a larger entropy loss due to significant changes in the six rotational degrees of freedom (three lost to vibrations, three altered) as well as the three translational entropies (lost to vibrations). It is not straightforward to derive ΔS_A from the B3LYP SCRF calculation, because the solvation effect (from the CSM) is not formally separable into entropy vs enthalpy components. However, if we assume that the CSM is applying a basic Trouton-like solvation entropy,⁶¹ we can estimate the ΔS_A as follows:

$$\begin{aligned} \Delta S_A &= \Delta S_A^{\text{gas}} + \Delta_A(\Delta S^{\circ \rightarrow *}) + \Delta_A \Delta_{\text{solv}} S \\ &\approx (-35 \pm 3) - R \ln(1000/24466) - R \ln(0.63/200) \\ &= (-35 \pm 3) + 64 + 11.4 \\ &= -17 \pm 3 \text{ cal mol}^{-1} \text{ K}^{-1}. \end{aligned} \quad (14)$$

In this estimate, the $\Delta S_A^{\text{gas}} \approx (-35 \pm 3)$ came from the consistent B3LYP frequency results for all the hydrogen bonded associations [Eqs. (7)–(10)], the 0.63 mL from free volume theory applied to the Trouton constant,⁶¹ and the 200 mL a rough midpoint for the molar volume of these “kite” liquids $B(\text{HA})_n$.

This constant value of $\Delta S_A = -17$ cal mol⁻¹ K⁻¹ is now taken to replace the Fuoss estimate [Eq. (13)] for each of the hydrogen-bond-forming associations [Eqs. (7)–(10)] in these acid-base mixtures. It corresponds to an effect of $-\Delta S = +5$ kcal mol⁻¹ in the Gibbs energy of association.

C. Enthalpy of association ΔH_A

Of the four relevant associations [Eqs. (7)–(10)], the enthalpy from the Fuoss K_A [Eq. (12)] only applies to the ion-pair association, and as the quantum-chemistry computed data reveals, even this association, which involves a large polyatomic anion $[\text{A}(\text{HA})_n^-]$, contains a significant contribution from the polarization of the anion, for which we shall add an ion-induced-dipole term [Eq. (15) below]. We also provide below similarly motivated new equations

TABLE V. Contributions r_{ij} (Å) and μ_{ij} (Å e₀) for generating r_{ni} [Eq. (19)] and $\mu_{n,i}$ [Eq. (20)] for ΔG_A prediction.

Contribution	Mixed-ESM ^a	Pure-B3LYP
r_{+1}	2.35	4.08
r_{+2}	-0.44	-0.33
r_{+3}	-0.60	-2.29
r_{+4}	2.76	4.21
r_{+5}	-0.20	-0.14
r_{+6}	-1.43	-2.88
r_{01}	2.34	2.15
r_{02}	-0.41	-0.37
r_{03}	0	0
r_{04}	1.25	1.62
r_{05}	-0.15	-0.27
r_{06}	0	0
μ_{+1}	1.45	2.90
μ_{+2}	-0.14	0.13
μ_{+3}	-0.99	-2.49
μ_{+4}	0.26	0.27
μ_{+5}	0	0
μ_{+6}	0	0
μ_{01}	1.52	2.53
μ_{02}	0.23	0.19
μ_{03}	-0.78	-2.43
μ_{04}	0.47	1.05
μ_{05}	0.20	-0.16
μ_{06}	0	0

^aFrom fitting to data (Figs. 2 and 3) that employed M06-2X/6-31+G(d,p)//B3LYP/6-31+G(d,p) electronic energies ($G_{el,e}^*$) and B3LYP/6-31+G(d,p) thermodynamic terms (G_{freq}^*) in Eq. (6).

for the other three associations [Eqs. (16)–(18)], using ion-induced dipole, ion-dipole, and dipole-induced-dipole terms. The computed data can be understood and reproduced by assuming the following electrostatic equations:

$$\Delta H_{A,+} = \frac{-N_{AVO}}{4\pi\epsilon_0\epsilon} \left(\frac{q_+\mu_{n,+}}{r_{n+}^2} + \frac{q_+q_-}{r_{n+}} \right), \quad (15)$$

$$\Delta H_{A,+0} = \frac{-N_{AVO}}{4\pi\epsilon_0\epsilon} \left(\frac{q_+\mu_{n,+}}{r_{n+}^2} \right), \quad (16)$$

$$\Delta H_{A,0-} = \frac{-N_{AVO}}{4\pi\epsilon_0\epsilon} \left(\frac{\mu_0\mu_{n,0}}{r_{n0}^3} + \frac{\mu_0q_-}{r_{n0}^2} \right), \quad (17)$$

$$\Delta H_{A,00} = \frac{-N_{AVO}}{4\pi\epsilon_0\epsilon} \left(\frac{\mu_0\mu_{n,0}}{r_{n0}^3} \right), \quad (18)$$

$$q_+ = q_- = e_0 \quad (\text{ion charge, } 1.602 \times 10^{-19} \text{ C}),$$

$$\mu_0 \approx (1 \text{ \AA}) * e_0 \quad (\text{dipole moment of AH}),$$

$$N_{AVO} e_0^2 / (4\pi\epsilon_0) = 332 \text{ \AA kcal mol}^{-1},$$

$$r_{ni} = (r_{i1} + r_{i2} \ln \epsilon + r_{i3} e^{-\zeta \Delta pK_a}) + n(r_{i4} + r_{i5} \ln \epsilon + r_{i6} e^{-\zeta \Delta pK_a}), \quad (19)$$

$$\mu_{n,i} = n(\mu_{i1} + \mu_{i2} \ln \epsilon + \mu_{i3} e^{-\zeta \Delta pK_a}) + n^2(\mu_{i4} + \mu_{i5} \ln \epsilon + \mu_{i6} e^{-\zeta \Delta pK_a}). \quad (20)$$

Here, the r_{ni} are the effective electrostatic distances from species i (BH⁺ if “+,” or AH if “0”) to the large species A(HA)_n[−] or B(HA)_n, and the $\mu_{n,i}$ are the effective dipole moments induced in A(HA)_n[−] or B(HA)_n by species i . These r_{ni} and $\mu_{n,i}$ values increase with kite length n , and likely depend slightly upon ϵ and ΔpK_a as well (perhaps smaller at higher ϵ and lower ΔpK_a). Hence, Eqs. (19) and (20) generate r_{ni} and $\mu_{n,i}$ values from the three variables (n , ϵ , and ΔpK_a) using additive contributions r_{ij} and μ_{ij} whose values were ultimately obtained from global fits of ΔG_A from Eqs. (14)–(20) to the 195 data points in Figs. 2 and 3. Six additive contributions were used for each of r_{n+} , r_{n0} , $\mu_{n,+}$, and $\mu_{n,0}$; a ΔpK_a scaling factor ζ (taken to be 0.02)

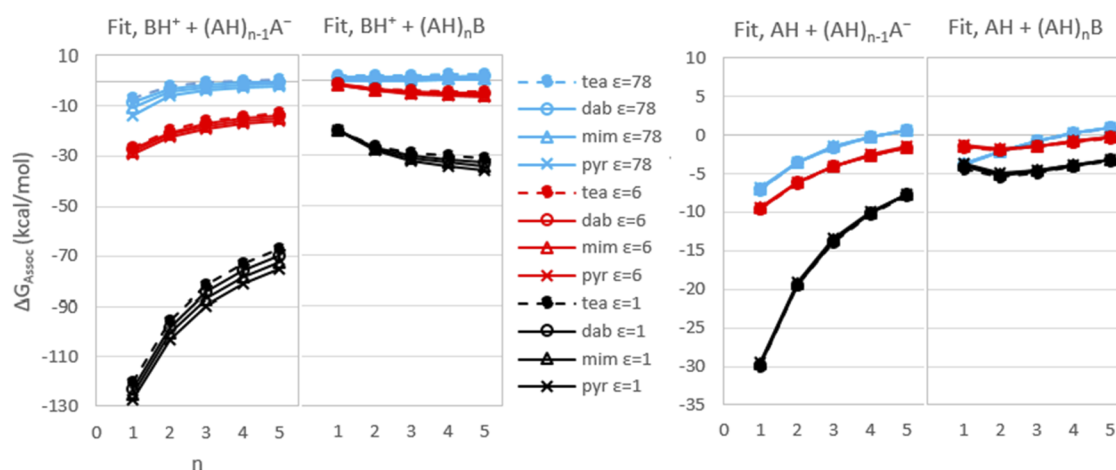


FIG. 5. Fitted-function results [Eqs. (14)–(20)] for all four associations [Eqs. (7)–(10)] using the mixed-ESM-fitted r -and- μ contributions set (Table V). The rms error relative to the computed data in Figs. 2 and 3 is 2.0 kcal mol^{−1}.

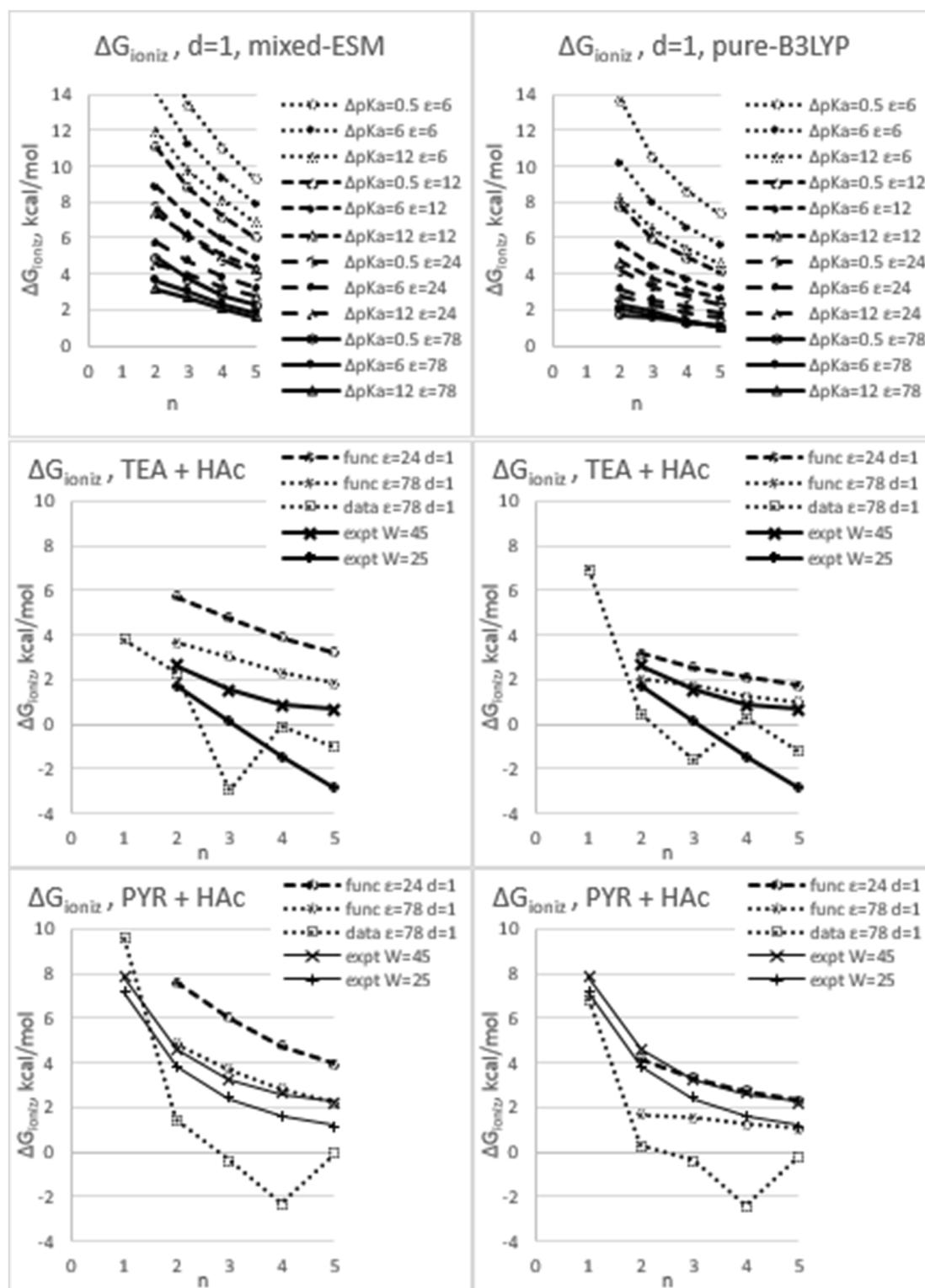


FIG. 6. Results for ΔG_{ioniz} from Eqs. (14)–(21); left and right columns using mixed-ESM and pure-B3LYP coefficients, respectively. Top row: plots showing predicted variation with ΔpK_a , ϵ , and n . Middle row: various results for trimethylamine + acetic acid. Bottom row: various results for pyridine + acetic acid.

was also needed. One contributions set (called the mixed-ESM set) was obtained by fitting to the 195 points in Figs. 2 and 3, which use M06-2X/6-31+G(d,p) for the $G_{el,\epsilon}^*$ electronic term in Eq. (6). A second contributions set (called the pure-B3LYP set) was obtained by fitting to an original sister dataset of 195 points obtained from using B3LYP/6-31+G(d,p) for $G_{el,\epsilon}^*$. Both contribution sets are provided in Table V, and the resulting functions achieved very good agreement (rms error 2.0 kcal mol⁻¹) with the original datasets. These functions with the pure-B3LYP contribution set have already been used in a follow-up paper probing BH⁺ stability in these systems.⁶⁵

Using the mixed-ESM contributions set in Table V, the resulting ΔG_A values from Eqs. (14)–(20) are plotted in Fig. 5. Tables of the r_{n+} , r_{n0} , $\mu_{n,+}$, and $\mu_{n,0}$ are provided in the [supplementary material](#).

To recap: these ΔH_A (and thus ΔG_A) expressions, with the recommended mixed-ESM-fitted r - and μ -contributions set, are functions of only three properties: the acid/base mixing ratio n , the acid-to-base proton-transfer strength ΔpK_a , and the dielectric constant ϵ . The dependence upon ΔpK_a is assumed to be upon the $\mu_{n,i}$ and r_{ni} [Eqs. (19) and (20)], and the use of the form $e^{-0.02\Delta pK_a}$ assures that there is a finite limit for the ΔG_A as ΔpK_a becomes infinitely large. The dependence upon ϵ is primarily the $1/(4\pi\epsilon_0\epsilon)$ factor [Eqs. (15)–(18)], with smaller effects upon $\mu_{n,i}$ and r_{ni} [Eqs. (19) and (20)]. Finally, the dependence upon the acid-base mixing ratio n [controlling the initial length of the ion-pair kites $B(HA)_n$] was chosen in a way that provides finite nonzero $n \rightarrow \infty$ asymptotes for $\Delta H_{A,+}$ and $\Delta H_{A,+0}$.

V. DISCUSSION: PIL AUTOIONIZATION

Using Eqs. (14)–(20), we can generate equations for the crucial autoionization equilibrium ΔG_{ioniz} , taking disproportionation $d = 1$ [see Eq. (11)],

$$\begin{aligned} \Delta G_{ioniz}(n; d = 1) = & -\Delta G_{A,\pm}(n + 1) + \Delta G_{A,+0}(n - 1) \\ & - \Delta G_{A,00}(n - 1) + \Delta G_{A,00}(n). \end{aligned} \quad (21)$$

The results from these predictive functions are plotted in Fig. 6. The upper-row plots in the figure show the variation of ΔG_{ioniz} with the three variables (mixing ratio n , dielectric constant ϵ , and acid/base strength parameter ΔpK_a). ΔG_{ioniz} is lowered by increasing any of these three variables, since these increase ion stability.

The remaining four plots show the degree of agreement with experimental conductivity-derived values known for $B = \text{tea}$ (middle-row plots) and $B = \text{pyr}$ (bottom-row plots). Two experimental curves are presented per system (solid curves) due to the uncertainty in the choice of the Walden constant W that relates conductivity to ion concentration. The dielectric constant value in the experimental systems is thought to be 20–30 for $n = 2$ –5 based on data by Orzechowski and co-workers,^{63,64} hence the provision of $\epsilon = 24$ function predictions (dashed curves). These dashed-line $\epsilon = 24$ predictions with the mixed-ESM coefficient set (left-hand plots) are higher than the experiment, which could be blamed on the small fitting errors, since for $\epsilon = 78$ (dotted curves), the function (circled points) is overpredicting the mixed-ESM training data (squared points). The dashed-line $\epsilon = 24$ predictions with the pure-B3LYP coefficient set (right-hand plots) are closer to the experiment, apparently due to lower fitting errors.

These predictive functions, fitted to quantum-chemistry computed data, appear to have succeeded in the dual goals of (i) predicting ΔG_{ioniz} (and hence degree of ionicity) as a function of three variables, including mixing ratio n , and (ii) revealing the underlying physics that controls such values. The pure-B3LYP coefficient set appears at the moment to be better than the mixed-ESM set for predicting ΔG_{ioniz} . Future work is already planned to extend the range of applicability of these functions to higher ΔpK_a values, of relevance to modern systems made from stronger acids.

VI. CONCLUSIONS

Quantum-chemistry continuum-solvation-model computations of Gibbs energies of association reveal that the ion-pairing Gibbs energy ΔG_{ioniz} , which controls ionicity in “poor” protic ionic liquids (made from weak acids and bases), is not predicted accurately by the Fuoss equation due to the need to account for anion polarization. With the inclusion of polarization (ion-to-induced-dipole) enthalpy terms, the quantum-chemistry data are better understood. Summary equations have been provided, which allow the prediction of ΔG of several associations and net autoionization, given only three variables: the mixing ratio n , the dielectric constant ϵ , and the acid-to-base proton-transfer strength parameter ΔpK_a . An initial comparison to experimental values for net autoionization (derived from published conductivity measurements) is quite good when using one of the two suggested coefficient sets. Future work will test the applicability of these functions to (i) conductivity predictions vs mixing ratio n , including consideration of a varying dielectric constant $\epsilon(n)$, and (ii) modern systems with greater ΔpK_a values made from stronger acids.

SUPPLEMENTARY MATERIAL

The details regarding the challenging geometry optimizations and tables of the values of the radii and induced dipole moments generated from Eqs. (19) and (20) are reported in the [supplementary material](#).

ACKNOWLEDGMENTS

This work was supported by the NSERC Canada (Grant No. RGPIN-2017-06247), with supercomputer funding from the CFI Canada (Grant No. LEF 2009-21625), and ISF Saskatchewan. R. Hempelmann (Saarland University) is thanked for his hospitality and office resources during ALLE’s sabbatical visit, during which much of the B3LYP data finalization and analysis was done. C. M. Nguyen and S. S. Rana (University of Regina) are thanked for their assistance with the testing of ΔG_A functions.

AUTHOR DECLARATIONS

Conflict of Interest

The authors have no conflicts to disclose.

Author Contributions

Devin O. Klapatiuk: Investigation (supporting). **Shawn L. Waugh:** Investigation (supporting). **Abdulrahman A. Mukadam:**

Investigation (supporting). **Allan L. L. East**: Conceptualization (lead); Data curation (lead); Formal analysis (lead); Funding acquisition (lead); Investigation (lead); Methodology (lead); Project administration (lead); Resources (lead); Software (lead); Supervision (lead); Validation (lead); Visualization (lead); Writing – original draft (lead); Writing – review & editing (lead).

DATA AVAILABILITY

The Cartesian coordinates from the myriad of Gaussian 09 runs that support the findings of this study are available from the corresponding author upon reasonable request.

REFERENCES

- M. Yoshizawa, W. Xu, and C. A. Angell, *J. Am. Chem. Soc.* **125**, 15411 (2003).
- C. A. Angell, N. Byrne, and J.-P. Belieres, *Acc. Chem. Res.* **40**, 1228 (2007).
- T. L. Greaves and C. J. Drummond, *Chem. Rev.* **108**, 206 (2008).
- T. L. Greaves and C. J. Drummond, *Chem. Rev.* **115**, 11379 (2015).
- D. R. MacFarlane, M. Forsyth, E. I. Izgorodina, A. P. Abbott, G. Annat, and K. Fraser, *Phys. Chem. Chem. Phys.* **11**, 4962 (2009).
- K. Ueno, H. Tokuda, and M. Watanabe, *Phys. Chem. Chem. Phys.* **12**, 1649 (2010).
- W. Xu, E. I. Cooper, and C. A. Angell, *J. Phys. Chem. B* **107**, 6170 (2003).
- S. K. Davidowski, F. Thompson, W. Huang, M. Hasani, S. A. Amin, C. A. Angell, and J. L. Yarger, *J. Phys. Chem. B* **120**, 4279 (2016).
- M. Hasani, S. A. Amin, J. L. Yarger, S. K. Davidowski, and C. A. Angell, *J. Phys. Chem. B* **123**, 1815 (2019).
- A. Noda, K. Hayamizu, and M. Watanabe, *J. Phys. Chem. B* **105**, 4603 (2001).
- H. Tokuda, S. Tsuzuki, M. A. B. H. Susan, K. Hayamizu, and M. Watanabe, *J. Phys. Chem. B* **110**, 19593 (2006).
- M. S. Miran, M. Hoque, T. Yasuda, S. Tsuzuki, K. Ueno, and M. Watanabe, *Phys. Chem. Chem. Phys.* **21**, 418 (2019).
- J. P. Hansen and I. R. McDonald, *Phys. Rev. A* **11**, 2111 (1975).
- K. Compaan and Y. Haven, *Trans. Faraday Soc.* **52**, 786 (1956).
- K. Compaan and Y. Haven, *Trans. Faraday Soc.* **54**, 1498 (1958).
- G. E. Murch, *Solid State Ionics* **7**, 177 (1982).
- M. C. Lonergan, J. W. Perram, M. A. Ratner, and D. F. Shriver, *J. Chem. Phys.* **98**, 4937 (1993).
- M. J. Monteiro, F. F. C. Bazito, L. J. A. Siqueira, M. C. C. Ribeiro, and R. M. Torresi, *J. Phys. Chem. B* **112**, 2102 (2008).
- T. Frömling, M. Kunze, M. Schönhoff, J. Sundermeyer, and B. Roling, *J. Phys. Chem. B* **112**, 12985 (2008).
- N. A. Stolwijk and S. Obeidi, *Electrochim. Acta* **54**, 1645 (2009).
- S. K. Mann, S. P. Brown, and D. R. MacFarlane, *ChemPhysChem* **21**, 1444 (2020).
- K. R. Harris, *J. Phys. Chem. B* **123**, 7014 (2019).
- J. O'M. Bockris and A. K. N. Reddy, *Modern Electrochemistry: Vol. 1. Ionics*, 2nd ed. (Plenum Press, New York, 1998).
- W. D. Compton, *Phys. Rev.* **101**, 1209 (1956).
- J. Bardeen and C. Herring, in *Imperfections in Nearly Perfect Crystals*, edited by W. Shockley (Wiley, New York, 1952), p. 261.
- H. Sato and R. Kikuchi, *J. Chem. Phys.* **55**, 677 (1971).
- R. Kikuchi and H. Sato, *J. Chem. Phys.* **55**, 702 (1971).
- A. Z. Borucka, J. O'M. Bockris, and J. A. Kitchener, *J. Chem. Phys.* **24**, 1282 (1956).
- A. Z. Borucka, J. O'M. Bockris, and J. A. Kitchener, *Proc. R. Soc. London, Ser. A* **241**, 554 (1957).
- W. Zhao, F. Leroy, B. Heggen, S. Zahn, B. Kirchner, S. Balasubramanian, and F. Müller-Plathe, *J. Am. Chem. Soc.* **131**, 15825 (2009).
- A. A. Lee, D. Vella, S. Perkin, and A. Goriely, *J. Phys. Chem. Lett.* **6**, 159 (2015).
- A. Klemm, *Z. Naturforsch.* **8a**, 397 (1953).
- R. W. Laity, *Ann. N. Y. Acad. Sci.* **79**, 997 (1960).
- B. Berne and S. A. Rice, *J. Chem. Phys.* **40**, 1347 (1964).
- K. R. Harris, *J. Phys. Chem. B* **120**, 12135 (2016).
- O. Hollóczki, F. Malberg, T. Welton, and B. Kirchner, *Phys. Chem. Chem. Phys.* **16**, 16880 (2014).
- B. Kirchner, F. Malberg, D. S. Firaha, and O. Hollóczki, *J. Phys.: Condens. Matter* **27**, 463002 (2015).
- F. Philippi, D. Rauber, M. Springborg, and R. Hempelmann, *J. Phys. Chem. A* **123**, 851 (2019).
- F. Philippi, A. Quinten, D. Rauber, M. Springborg, and R. Hempelmann, *J. Phys. Chem. A* **123**, 4188 (2019).
- Y. Shao, K. Shigenobu, M. Watanabe, and C. Zhang, *J. Phys. Chem. B* **124**, 4774 (2020).
- F. Philippi, K. Goloviznina, Z. Gong, S. Gehrke, B. Kirchner, A. A. H. Pádua, and P. A. Hunt, *Phys. Chem. Chem. Phys.* **24**, 3144 (2022).
- T. I. Morrow and E. J. Maginn, *J. Phys. Chem. B* **106**, 12807 (2002).
- B. L. Bhargava and S. Balasubramanian, *J. Chem. Phys.* **127**, 114510 (2007).
- E. J. Maginn, *J. Phys.: Condens. Matter* **21**, 373101 (2009).
- C. Schreiner, S. Zugmann, R. Hartl, and H. J. Gores, *J. Chem. Eng. Data* **55**, 1784 (2010).
- W. M. Haynes, D. R. Lide, and T. J. Bruno, *CRC Handbook of Chemistry and Physics: A Ready-Reference Book of Chemical and Physical Data*, 97th ed. (CRC Press, Boca Raton, FL, 2016, 2017).
- H. E. Patten, *J. Phys. Chem.* **6**, 554 (1902).
- L. E. Swearingen and R. F. Ross, *J. Phys. Chem.* **38**, 1141 (1934).
- P. Huyskens, N. Felix, A. Janssens, F. Van den Broeck, and F. Kapuku, *J. Phys. Chem.* **84**, 1387 (1980).
- F. Kohler, R. Gopal, G. Goetze, H. Atrops, M. A. Demeriz, E. Liebermann, E. Wilhelm, F. Ratkovic, and B. Palagyi, *J. Phys. Chem.* **85**, 2524 (1981).
- R. G. Treble, K. E. Johnson, and E. Tosh, *Can. J. Chem.* **84**, 915 (2006).
- N. P. Aravindakshan, K. E. Gemmell, K. E. Johnson, and A. L. L. East, *J. Chem. Phys.* **149**, 094505 (2018).
- D. O. Klapatiuk, K. E. Johnson, and A. L. L. East, *ECS Trans.* **98**, 149 (2020).
- R. M. Fuoss and C. A. Kraus, *J. Am. Chem. Soc.* **55**, 2387 (1933).
- Y. Miyauchi, M. Hojo, N. Ide, and Y. Imai, *J. Chem. Soc., Faraday Trans.* **88**, 1425 (1992).
- R. M. Fuoss, *J. Am. Chem. Soc.* **80**, 5059 (1958).
- M. J. Frisch, G. W. Trucks, H. B. Schlegel, G. E. Scuseria, M. A. Robb, J. R. Cheeseman, G. Scalmani, B. Varone, B. Mennucci, G. A. Petersson, H. Nakatsuji, M. Caricato, X. Li, H. P. Hratchian, A. F. Izmaylov, J. Bloino, G. Zheng, J. L. Sonnenberg, M. Hada, M. Ehara, K. Toyota, R. Fukuda, J. Hasegawa, M. Ishida, T. Nakajima, Y. Honda, O. Kitao, H. Nakai, T. Vreven, J. A. Montgomery, Jr., J. E. Peralta, F. Ogliaro, M. Bearpark, J. J. Heyd, E. Brothers, K. N. Kudin, V. N. Staroverov, R. Keith, R. Kobayashi, J. Normand, K. Raghavachari, A. Rendell, J. C. Burant, S. S. Iyengar, J. Tomasi, M. Cossi, N. Rega, J. M. Millam, M. Klene, J. E. Knox, J. B. Cross, V. Bakken, C. Adamo, J. Jaramillo, R. Gomperts, R. E. Stratmann, O. Yazyev, A. J. Austin, R. Cammi, C. Pomelli, J. W. Ochterski, R. L. Martin, K. Morokuma, G. Zakrzewski, G. A. Voth, P. Salvador, J. J. Dannenberg, S. Dapprich, A. D. Daniels, O. Farkas, J. B. Foresman, J. V. Ortiz, J. Cioslowski, and D. J. Fox, Gaussian 09, Rev. C01, Gaussian, Inc., Wallingford, CT, 2010.
- J. Tomasi, B. Mennucci, and E. Cancès, *J. Mol. Struct.: THEOCHEM* **464**, 211 (1999).
- M. Cossi, G. Scalmani, N. Rega, and V. Barone, *J. Chem. Phys.* **117**, 43 (2002).
- K. Rappé, C. J. Casewit, K. S. Colwell, W. A. Goddard III, and W. M. Skiff, *J. Am. Chem. Soc.* **114**, 10024 (1992).
- D. H. Patel and A. L. L. East, *J. Phys. Chem. A* **124**, 9088 (2020).
- D. Fox, private communication (2018); F. Clemente, private communication (2021).
- K. Orzechowski, M. Pajdowska, J. Przybylski, J. Gliński, and H. A. Kołodziej, *Phys. Chem. Chem. Phys.* **2**, 4676 (2000).
- K. Orzechowski, M. Pajdowska, K. Fuchs, and U. Kaatze, *J. Chem. Phys.* **119**, 8558 (2003).
- S. S. Rana and A. L. L. East, *ECS Trans.* **109**, 11 (2022).